

Observation of the thermal acoustic breathing modes of a bubble

K. G. SCHEUER,¹ F. B. ROMERO,² AND R. G. DECORBY^{2*}

¹*Ultracoustics Technologies Ltd., Sherwood Park, AB, Canada, T8A 3H5*

²*ECE Department, University of Alberta, 9211-116 St. NW, Edmonton, AB, Canada, T6G 1H9*

**Corresponding author: rdecorby@ualberta.ca*

We report experimental observations of the volume acoustic modes of air bubbles in water, including both the fundamental Minnaert breathing mode and a family of higher-order modes extending into the megahertz frequency range. Bubbles were placed on or near optomechanical sensors having a noise floor substantially determined by ambient medium fluctuations, and thus able to detect thermal Brownian motions of proximate objects. Bubble motions could be coupled to the sensor through both air (*i.e.*, with the sensor inside the bubble) and water, verifying that sound is radiated by the high-order modes. In some cases, we also observed hybridization between the mechanical modes of the sensor and those of nearby bubbles. Finally, and more speculatively, we found evidence for Purcell-effect modification of the sensor vibrational spectrum when encapsulated by a bubble.

DOI: XXX

Owing in large part to their inherent beauty and transient nature, bubbles have long been a source of fascination [1]. They also host rich physics, with important technological implications [2], especially regarding their interactions with acoustic waves. Natural oscillations of entrained gas bubbles produce audible signals, such as the familiar sound of running water [2,3]. When they are actively driven by an external pressure wave, the cyclic collapse of bubbles can result in extremely energetic processes such as the cavitation-induced damage of solid objects [2]. Other phenomena associated with bubble cavitation include the emission of light, (*i.e.*, sonoluminescence [4]) and the catalysis of reactions (*i.e.*, sonochemistry [5]). Moreover, there is growing interest in bubble-mediated nonlinear interactions between phonons and photons [6]. For such a common-place object, they continue to attract a remarkable amount of research.

Many acoustic properties of bubbles can be explained in terms of the well-known Minnaert ‘breathing mode’ [1,3,7]. For a spherical air-bubble in water at atmospheric pressure, for example, the resonant frequency of this mode can be approximated as $f_M \sim 3.3/R$, where R is the radius of the bubble. It follows that the associated acoustic wavelength (in both air and water) is much larger than the bubble dimensions ($\lambda \gg R$) [3]. In fact, the Minnaert breathing mode is the lowest-order solution of the so-called Rayleigh-Plesset (RP) equation [7], which (*a priori*) assumes that the pressure inside the bubble is a spatially uniform function of time only. The RP equation also permits higher-order solutions – known as ‘shape modes’ [2,8] – which are essentially capillary modes

mediated by surface tension. These shape modes do not interact strongly with an acoustic radiation field [2], at least not within a linear approximation [9].

Minnaert’s original derivation effectively treated the bubble as a mass-spring system, where the compression/rarefaction of the confined gas plays the role of the spring and the inertia of the surrounding liquid contributes the mass. However, from a higher level perspective, a bubble might be viewed as an elastic body (the gas sphere) bounded by a viscous, compressible fluid. Alternatively, one can think of the bubble as an enclosure or ‘room’ [10] within a homogeneous fluid medium. In either case, one would then expect a bubble to support a family of volume acoustic modes, for which the pressure (and related parameters) inside the bubble are functions of both time *and position*. The volume modes of small bubbles are expected to occur at very high ultrasonic frequencies and would thus be subject to higher acoustic attenuation. Perhaps as a result, they have not been widely studied in the literature.

A notable exception is the theoretical work by Devaud *et al.* [3], who solved for a family of radial breathing modes, drawing an analogy to the Fabry-Perot modes of a spherical-mirror optical cavity. Remarkably, their work demonstrated that the Minnaert resonance is in fact the lowest-order mode within this set. Its low resonant frequency (*i.e.*, a wavelength much larger than the bubble dimensions) is attributed to the dispersion imparted by the curved bubble interface. An analogous effect can occur in optical cavities with dispersive mirrors [11].

While the higher-order acoustic modes are anticipated, and confirmed by Devaud’s work, to date there is a scarcity of experimental evidence. Here, we report direct observation of these high-order volume breathing modes in the ~1-10 MHz ultrasonic range, for single tethered bubbles coupled to on-chip optomechanical sensors [12]. The noise floor of these sensors is determined mainly by thermomechanical noise, and in fact they are very nearly ambient-medium-noise-limited [13-16] over a wide frequency range. As a result, resonant vibrational energy confined within the acoustic modes of the bubble, and driven only by Brownian motion, is imprinted directly on the noise of the sensor. The measured acoustic mode spectrum, for a range of bubble sizes, is shown to be in good agreement with numerical predictions. We also provide evidence that these high-frequency modes are coupled to propagating acoustic waves.

To provide context, we start by considering the archetypal case of a spherical air bubble in a water medium. As mentioned, Devaud *et al.* [3] provided a quasi-analytical derivation of the radially symmetric volume modes for this system. Inside the air bubble, these modes can be expressed as $p(r) = (A/r) \cdot \sin(q_a \cdot r)$, where p is pressure, r is the radial coordinate, A is a constant amplitude, $q_a = (\omega/c)$ is the wave number, and c is the sound velocity in air. They furthermore showed that the resonant frequencies for a bubble of radius R can be expressed:

$$x_a = q_a R \approx 0.0623, 4.49, 7.73, \dots \approx \frac{(2n+1)\pi}{2} . \quad [1]$$

The lowest-order resonance is the well-known Minnaert breathing mode, characterized by a nearly homogeneous internal pressure. The others are higher-order, radially symmetric breathing modes. Notably, the first higher-order (radially symmetric) resonance is predicted to lie at ~ 72x higher frequency than the fundamental Minnaert resonance. As an example, for a typical millimeter-scale air bubble in water with Minnaert frequency $f_M \sim 10$ kHz, this places the next radial resonance at ~ 720 kHz.

A simpler model would treat the bubble as an “acoustic room” with hard boundaries [10], an approximation which can be justified by the large acoustic impedance mismatch between the air and the water, and between the air and the underlying substrate for a tethered bubble. While Flanagan’s solutions are for a hemispherical room [10], they can be extended to the full sphere by invoking image theory since the equatorial plane is a perfectly reflecting hard boundary. In this simple system, the air cavity hosts pure eigen-modes with pressure distribution given by:

$$p(r, \theta, \varphi, t) \sim \left\{ \frac{\sin}{\cos}(m\varphi) \right\} \cdot \{L_l^m(\cos \theta)\} \cdot \left\{ J_l \left(\frac{\omega l n r}{c} \right) \right\} , \quad [2]$$

where φ and θ are the azimuthal and polar angles, respectively, L_l^m is a Legendre function of the first kind (degree l , order m) defined in Ref. [10], and J_l is a spherical

Bessel function. The resonance frequencies are determined by the positive integers l and n , and the modes are degenerate for values of the positive integer m ($m \leq l$). Solutions include a subset of purely radial modes:

$$p_n(r) \sim J_0 \left(\frac{\omega_{0n} r}{c} \right) = \sin \left(\frac{\omega_{0n} r}{c} \right) / \left(\frac{\omega_{0n} r}{c} \right) , \quad [3]$$

where $\omega_{0n} = \{0, 4.5, 7.8, \dots\} \cdot c/R$ are the radial-mode eigen-frequencies in good agreement with Eq. (1). However, the two lowest-order (non-static) modes are actually non-radial, including the lowest-order mode:

$$p_{111}(r, \theta, \varphi) \sim \cos \varphi \cdot \sin \theta \cdot j_1 \left(\frac{\omega_{11} r}{c} \right) , \quad [4]$$

with $\omega_{11} = 2.0 \cdot c/R$.

This “acoustic room” analogy produces good agreement with the predictions of a numerical solver. Specifically, we modeled the air-bubble-in-water system using the ‘Pressure Acoustics’ module in COMSOL Multiphysics. For simplicity, the air and water were assigned fixed sound velocities (330 and 1500 m/s, respectively) and absorption was neglected. Further details of the simulation, including boundary conditions, are provided in the supplementary information file.

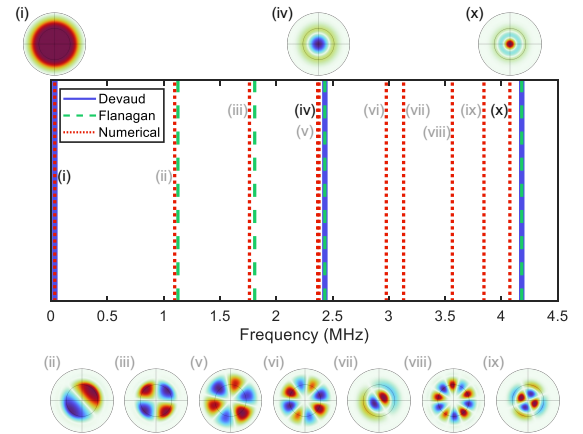


FIG. 1. The predicted eigen-frequencies for the acoustic modes of a 100- μ m-radius bubble are indicated by the vertical lines. Results from a numerical solver (COMSOL), an analytical bubble model for radial modes only [3], and an analytical model for an “acoustic room” with hard walls [10] are indicated by the legend. The numerically predicted pressure distributions for the ten lowest-order modes are also shown, with the gas/liquid boundary indicated by the inner concentric circle. The mode labeled as ‘(i)’ is the Minnaert breathing mode, and the others are higher-order acoustic modes.

The predictions of the analytical and numerical models are compared in Fig. 1 and show very good overall agreement. Slight discrepancies between the analytical and numerical results can be attributed to differences in the treatment of the boundary conditions as well as numerical error arising from the finite mesh size and simulation volume. Aside from this, there is nearly perfect agreement (for the higher-order modes)

between the numerical and ‘acoustic room’ [10] models, including the ordering and pressure profiles of the modes. The Minnaert resonance, which is not captured by the hard-boundary model, is well-predicted by the other two models.

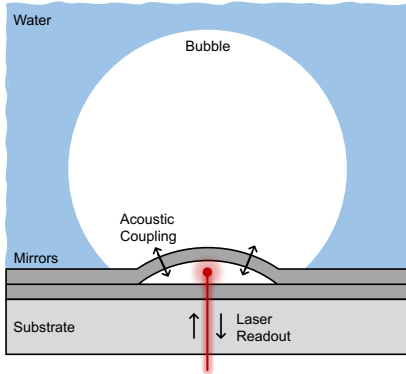


FIG. 2. Schematic cross-sectional view of a tethered bubble centered over a buckled dome Fabry-Perot optomechanical sensor. The motion of the flexible upper mirror is imprinted onto the laser light reflected from the optical cavity. The motion of the bubble is detected via the effect it has on the mirror motion.

We turn our attention next towards the experimental observation of these breathing modes. This was achieved by placing a tethered bubble over an optomechanical sensor, effectively positioning a sensor inside a bubble, as illustrated in Fig. 2. Sensor chips were first covered with a ‘‘puddle’’ of DI water and then air bubbles were injected using a syringe and needle [8]. A technique was developed for accurately positioning a bubble over an individual sensor, by first tethering it to the substrate plane and then dragging it with the dispensing needle. A video demonstrating this process has been included as supplementary information.

The optomechanical sensors used here are 100- μm -diameter ‘buckled dome’ Fabry-Perot cavities, described in detail elsewhere [12]. The upper buckled mirror functions as the mechanical oscillator, and its vibrational motion is imprinted on the light reflected from an interrogation laser tuned near an optical cavity resonance. As mentioned above, these sensors operate at the thermomechanical noise limit [14] with a significant contribution from ambient medium noise [16]. As a result, they are exquisitely sensitive to their local environment [17,18]. For the measurements described below, the reflected laser light was delivered to a high-speed photodetector and power spectral density (PSD) plots were generated from sampled noise signals. The laser power is sufficiently low to ensure that back-action effects can be neglected, so that the laser is simply a passive probe of the vibrational motion of the mirror [18]. Further details concerning the experimental measurement scheme and data processing are provided in the supplementary information

file.

Results for a relatively small bubble ($R \sim 95 \mu\text{m}$) are shown in Fig. 3. The interrogation laser was coupled to a particular sensor, and sensor noise spectra were recorded at fixed laser power but with variations in the medium external to the sensor. The blue curve in Fig. 3(a) is the spectrum measured in ‘‘bulk’’ air, and it shows a typical [12] series of resonant peaks (e.g. at ~ 2.5 and 6 MHz) associated with the inherent vibrational modes of the buckled mirror. The red curve is the spectrum measured with a small, tethered air bubble positioned over the sensor as shown in Fig. 3(c). Clearly, the noise spectrum is modified relative to the bulk case, most apparently by the appearance of several new resonant peaks. These peaks are well correlated with the acoustic-mode eigen-frequencies of the tethered bubble as predicted by a COMSOL numerical model and indicated by the dashed vertical lines. The correspondingly predicted spatial pressure distributions are also shown, evincing strong analogies with the higher-order modes solved for the spherical bubble case above.

Slight discrepancies between the experimental and theoretical eigen-frequencies can be attributed to uncertainties in estimating bubble dimensions from the microscope images, and also to the neglect of hybridization between sensor and bubble vibrational modes in the numerical model. Nevertheless, the global alignment is very good, and was consistently observed across multiple bubble-sensor combinations (see Fig. 4 below and the SI file for additional examples), allowing us to confidently assert that these measurements are in fact revealing the high-frequency volume modes of the bubbles. While not easily seen in the wide-range plot, the Minnaert resonance was also imprinted on the noise spectrum of the sensor as shown in the zoomed-in plot of Fig. 3(b). The position of this resonance is in excellent agreement with the COMSOL model and also with analytical predictions [19] for a tethered bubble (see the SI file for additional discussion), and assuming a contact angle of 30 degrees as estimated from the microscope images. In this case, $f_{\text{TM}} \sim 0.83 \cdot f_{\text{M}}$ [19], where f_{TM} is the fundamental breathing mode of the tethered bubble of radius R .

Aside from the clear signatures of bubble acoustic modes, the data in Fig. 2 also contains compelling evidence that the vibrational spectrum of the optomechanical sensor is itself strongly modified. We attribute this to a significant modification of the local density of states (LDOS) in the acoustic environment of the sensor [20-22]. To draw an analogy with electromagnetic systems, the optomechanical sensor can be viewed as the ‘‘acoustic emitter’’ while the bubble represents an acoustic resonant cavity encapsulating the emitter.

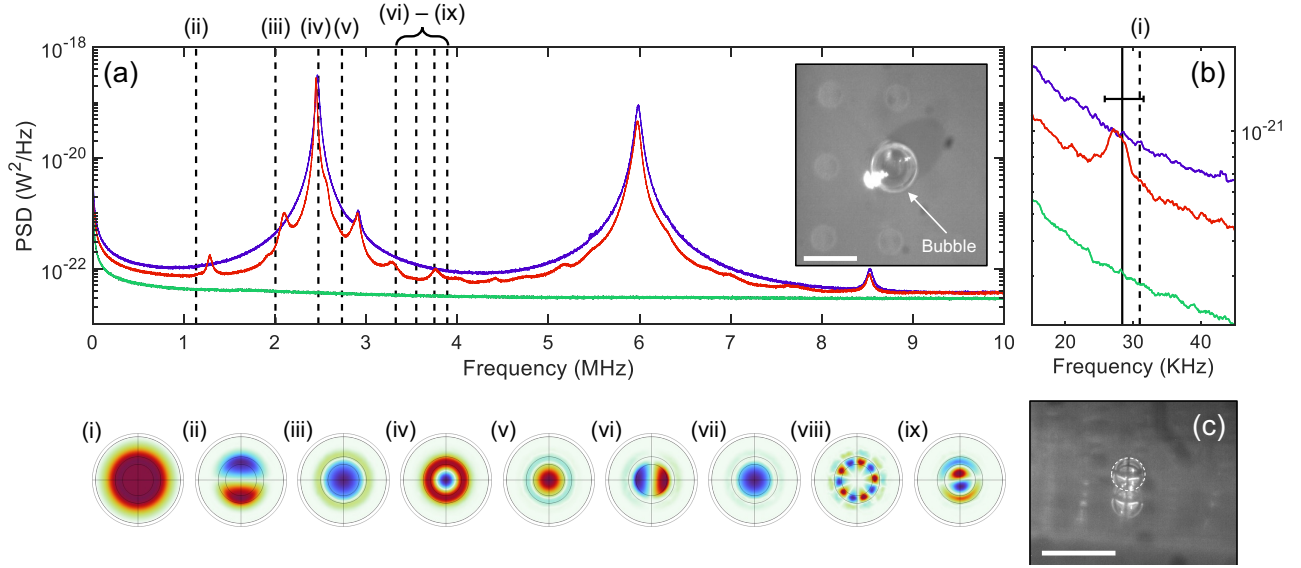


FIG. 3. (a) Power spectral densities for the same sensor in air (blue curve) and encapsulated by a bubble (red curve). The shot noise floor for the same average received power at the photodetector is also shown (green curve). The vertical dashed lines indicate numerically predicted eigen-frequencies for the lowest-order bulk acoustic modes of the bubble. Corresponding acoustic pressure distributions at the bubble/substrate interface are also shown. The innermost concentric circle is the contact line of the bubble, and the adjacent circle is its outer circumference. A top-down-view microscope image of the bubble and surrounding sensors is shown as the inset (scale bar – 200 μm). (b) A zoomed-in version of the data presented in (a), showing the Minnaert resonance near 30 KHz. Theoretical and numerical predictions are also plotted as solid and dashed vertical lines, respectively. The error bar represents a $\pm 10\%$ deviation in the estimated bubble diameter. (c) A side profile microscope image of the tethered bubble (scale bar – 500 μm).

Notably, the data reveal: i. a suppression/inhibition of background acoustic emission over nearly the entire ~ 1 -10 MHz range, except at bubble resonances, ii. a narrowing of the dominant “emission lines” at ~ 2.5 and 6 MHz, corresponding to an increase in the associated lifetimes, and iii. a slight red-shift of the “emitter” frequencies consistent with a cavity-modified Lamb-shift [22]. We observed similar behavior for multiple small-bubble/sensor combinations, and a more detailed example is provided in the SI file. These observations are consistent with a redistribution of the vibrational energy of the sensor, caused by the modified acoustic environment. The degree of modification is quite remarkable given the fact that the mechanical oscillator is coupled to other thermal baths, in particular the underlying substrate. It is further evidence that the noise floor of these sensors is substantially limited by their external medium [16]. A more complete study is left for future work.

Analogous results for a larger bubble ($R \sim 313 \mu\text{m}$) are shown in Fig. 4. Compared to the smaller bubble results, a much denser spectrum of higher-order acoustic modes is revealed (see Fig. 4(a)). As above, the noise spectrum contains a signature of the low-frequency Minnaert resonance, and its location is again in good agreement with predictions (see Fig. 4(b)). The acoustic mode spectrum of the bubble is further revealed by normalizing the data obtained with the bubble in place to the data obtained for the

bulk air case, as shown in Fig. 4(c). The numerically predicted eigen-frequencies of the six lowest-order acoustic modes, including the Minnaert resonance, are indicated by the dashed vertical lines, and show excellent alignment with the experimental peaks. Evidence of acoustic modes extending up to nearly 10 MHz is apparent, but assignment of individual modes becomes difficult due to the high density of modes predicted above ~ 1 MHz. The quality factor of the lower-order modes is as high as ~ 70 (see the SI file for further discussion), in good agreement with theoretical predictions considering radiation, thermal, and viscous damping [3]. We speculate that the lower quality of the modes above 1 MHz might in part be attributable to the dramatic rise of ultrasound attenuation in air for frequencies in this range [23]. Finally, we mention experiments aimed at observing the radiation of energy into the water medium. To this end, air bubbles were either tethered to the chip surface near (but not overtop of) a sensor of interest, or suspended from the needle in close proximity to the sensor of interest. In both cases, signatures of bubble acoustic modes were observed in the sensor noise spectrum (see the SI file for examples). These features are less prominent than those shown above, which is expected because only a fraction of the energy circulating inside the bubble is coupled externally. Nevertheless, the results confirm that these higher-order modes are exchanging energy with the external radiation field [3].

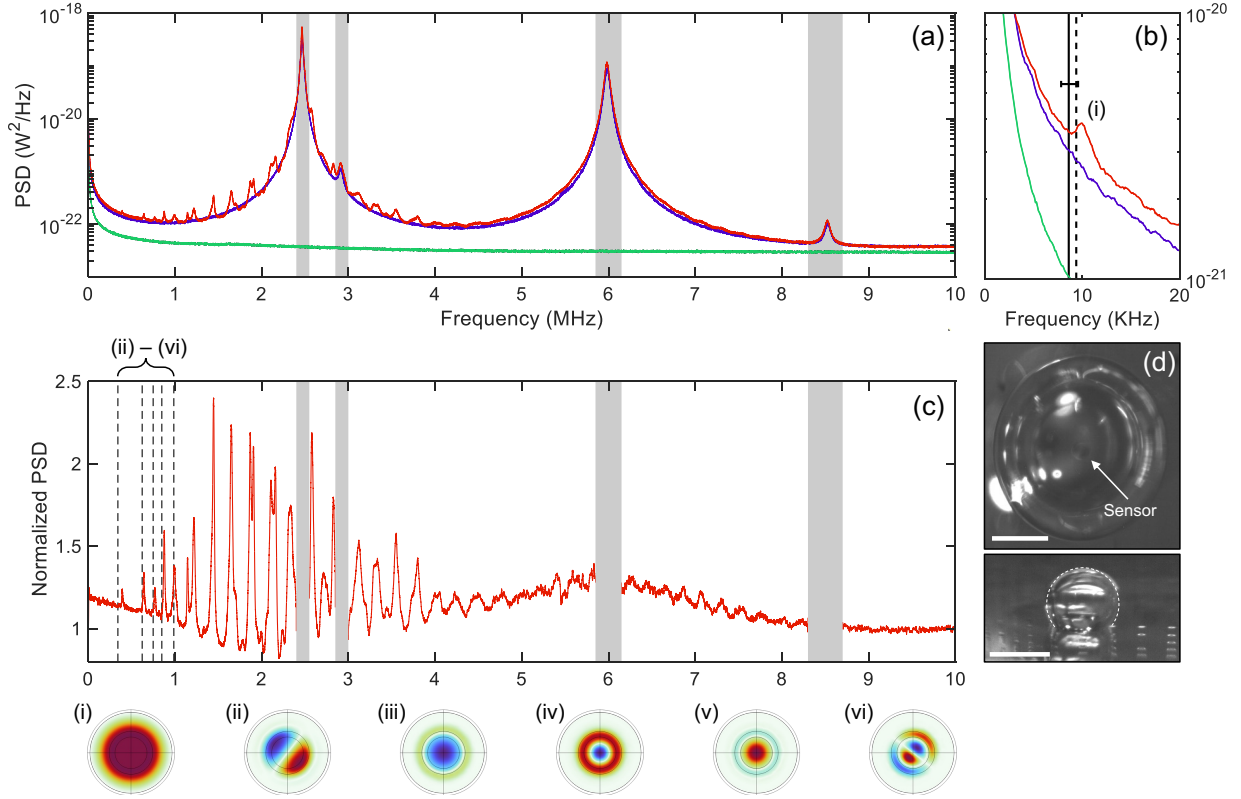


FIG. 4. Analogous results to those presented in Fig. 3 but for a larger bubble. (a) Power spectral densities showing the sensor in air (blue), encapsulated by a bubble (red), and the shot noise (green). The grey bands represent regions dominated by mechanical modes inherent to the sensor. (b) A zoomed version of the data presented in (a), showing the Minnaert resonance near 10 KHz. Theoretical and numerical predictions are also plotted as solid and dashed vertical lines, respectively. The error bar represents a $\pm 10\%$ deviation in the estimated bubble diameter. (c) A normalized version of the data in part a. is shown, to further isolate the acoustic modes of the bubble. The first 6 numerically predicted eigenfrequencies are also plotted as vertical dashed lines with their corresponding acoustic pressure distributions shown below the plot. (d) Microscope images showing the top and side views of the bubble (scale bars – 200 μm and 500 μm , respectively).

In summary, we described an experimental study of the acoustic resonances of air bubbles in water, for frequencies extending into the megahertz ultrasound range. The results illustrate that the vibrational properties of a bubble go beyond the Minnaert breathing mode and capillary modes predicted by the Rayleigh-Plesset equation. It would be fair to consider if these higher-order volume modes are mainly of theoretical interest, or rather might have practical implications. Undoubtedly, the situations where they are expected to be manifest are fewer than that for the Minnaert resonance, simply because of the increased attenuation of sound with frequency, especially in air. Moreover, the Minnaert resonance is unique in the sense that it involves prominent motion of the relatively massive water medium, which ties it more directly to the dramatic effects associated with acoustic cavitation. For the higher-order modes, their characteristic oscillation frequencies are such that the dominant motion is that of the gas molecules inside the bubble (*i.e.*, a standing pressure wave).

Nevertheless, the internal state and dynamics of a gas bubble is an incredibly complex physical problem, especially in scenarios involving the collapse of oscillating bubbles [7]. It seems plausible that any complete description will need to include consideration of the higher-order acoustic modes. Notably, energy storage by acoustic modes of a bubble has been posited as a potential contributor to the extreme conditions leading to single-bubble sonoluminescence [24], although the same authors subsequently discounted this theory [25] due to a lack of experimental corroboration (and consistent with the conclusions outlined in Geers *et al.* [26]). Notwithstanding this point of view, the role of acoustic modes remains a matter of ongoing debate [27]. Moreover, it is possible that higher-order acoustic breathing modes could play a role in emerging fields, including phonon-photon interactions mediated by bubbles [6,7] and the use of bubbles in biosensing and related applications [28-30]. In any case, it seems likely that the acoustics of bubbles will continue to yield new surprises.

This research was funded by the Government of Alberta (Innovation Catalyst Grant), Alberta Innovates, the Natural Sciences and Engineering Research Council of Canada (CREATE 495446-17), and the Alberta EDT Major Innovation Fund (Quantum Technologies).

1. A. Prosperetti, "Bubbles," *Phys. Fluids* **16**(6), 1852-1865 (2004).
2. T. G. Leighton, *The Acoustic Bubble*, Academic Press, London (1997).
3. M. Devaud, T. Hocquet, J.-C. Bacri, and V. Leroy, "The Minnaert bubble: an acoustic approach," *Eur. J. Phys.* **29**, 1263-1285 (2008).
4. C. Cairo and R. Mettin, "Simultaneous high-speed recording of sonoluminescence and bubble dynamics in multibubble fields," *Phys. Rev. Lett.* **118**, 064301 (2017).
5. K. S. Suslick, "Sonochemistry," *Science* **247**, 1439-1445 (1990).
6. I. S. Maksymov and A. D. Greentree, "Coupling light and sound: giant nonlinearities from oscillating bubbles and droplets," *Nanophotonics* **8**(3), 367-390 (2019).
7. W. Lauterborn and T. Kurz, "Physics of bubble oscillations," *Rep. Prog. Phys.* **73**, 106501 (2010).
8. Z. Zhang, Y. Wang, Y. Amarouchene, R. Boisgard, H. Kellay, A. Wurger, and A. Maali, "Near-field probe of thermal fluctuations of a hemispherical bubble surface," *Phys. Rev. Lett.* **126**, 174503 (2021).
9. Y. Mao, L. A. Crum, and R. A. Roy, "Nonlinear coupling between the surface and volume modes of an oscillating bubble," *J. Acoust. Soc. Am.* **98**, 2764-2771 (1995).
10. J. L. Flanagan, "Acoustic modes of a hemispherical room," *J. Acoust. Soc. Am.* **37**(4), 616-618 (1965).
11. E. Garmire, "Theory of quarter-wave-stack dielectric mirrors used in a thin Fabry-Perot filter," *Appl. Opt.* **42**(27), 5442-5449 (2003).
12. G. J. Hornig, K. G. Scheuer, E. B. Dew, R. Zemp, and R. G. DeCorby, "Ultrasound sensing at thermomechanical limits with optomechanical buckled-dome microcavities," *Opt. Express* **30**(18), 33083-33096 (2022).
13. R. H. Mellen, "The thermal noise limit in the detection of underwater acoustic signals," *J. Acoust. Soc. Am.* **24**(5), 478-480 (1952).
14. B.-B. Li, L. Ou, Y. Lei, and Y.-C. Liu, "Cavity optomechanical sensing," *Nanophotonics* **10**(11), 2799-2832 (2021).
15. A. M. Winkler, K. Maslov, and L. V. Wang, "Noise-equivalent sensitivity of photoacoustics," *J. Biomed. Opt.* **18**(9), 097003 (2013).
16. S. Basiri-Esfahani, A. Armin, S. Forstner, and W. P. Bowen, "Precision ultrasound sensing on a chip," *Nat. Commun.* **10**(1), 132 (2019).
17. G. J. Hornig, K. G. Scheuer, and R. G. DeCorby, "Observation of thermal acoustic modes of a droplet coupled to an optomechanical sensor," *Appl. Phys. Lett.* **123**, 042202 (2023).
18. K. G. Scheuer, F. B. Romero, G. J. Hornig, and R. G. DeCorby, "Ultrasonic spectroscopy of sessile droplets coupled to optomechanical sensors," arXiv (2023).
19. A. O. Maksimov, "On the volume oscillations of a tethered bubble," *J. Sound and Vibration* **283**, 915-926 (2005).
20. M. Landi, J. Zhao, W. E. Prather, Y. Wu, and L. Zhang, "Acoustic Purcell effect for enhanced emission," *Phys. Rev. Lett.* **120**, 114301 (2018).
21. M. K. Schmidt, L. G. Helt, C. G. Poulton, and M. J. Steel, "Elastic Purcell effect," *Phys. Rev. Lett.* **121**, 064301 (2018).
22. L. Langguth, R. Fleury, A. Alu, and A. F. Koenderink, "Drexhage's experiment for sound," *Phys. Rev. Lett.* **116**, 224301 (2016).
23. S. Takahashi, "Properties and characteristics of P(VDF/TrFE) transducers manufactured by a solution casting method for use in the MHz-range ultrasound in air," *Ultrasonics* **52**(3), 422-426 (2012).
24. M. P. Brenner, S. Hilgenfeldt, D. Lohse, and R. R. Rosales, "Acoustic energy storage in single bubble sonoluminescence," *Phys. Rev. Lett.* **77**(16), 3467-3470 (1996).
25. M. P. Brenner, S. Hilgenfeldt, and D. Lohse, "Single-bubble sonoluminescence," *Rev. Mod. Phys.* **74**, 425-484 (2002).
26. T. L. Geers, R. S. Lagumbay, and O. V. Vasilyev, "Acoustic-wave effects in violent bubble collapse," *J. Appl. Phys.* **112**, 054910 (2012).
27. Y. Q. Yu and Z. Zong, "A study of the internal vibration of a single oscillating bubble," *Phys. Fluids* **33**, 076106 (2021).
28. A. Hashmi, G. Yu, M. Reilly-Collette, G. Heiman, and J. Xu, "Oscillating bubbles: a versatile tool for lab on a chip applications," *Lab Chip* **12**, 4216-4227 (2012).
29. T. Segers and M. Versluis, "Acoustic bubble sorting for ultrasound contrast agent enrichment," *Lab Chip* **14**, 1705-1714 (2014).
30. I. S. Maksymov, B. Q. H. Nguyen, and S. A. Suslov, "Biochemical sensing using gas bubble oscillations in liquids and adjacent technologies: theory and practical applications," *Biosensors* **12**, 624 (2022).